JOURNAL OF GEOPHYSICAL RESEARCH, VOL. 105, NO. B6, PAGES 13,655–13,673, JUNE 10, 2000

An analysis of large-scale variations in small-scale mantle heterogeneity using Global Seismographic Network recordings of precursors to *PKP*

Michael A. H. Hedlin and Peter M. Shearer
Institute of Geophysics and Planetary Physics, Scripps Institution of Oceanography
University of California, San Diego, La Jolla

Abstract. High-frequency precursors to the core phase *PKP* are caused by scattering off heterogeneities in the lowermost mantle and D″ regions, and they provide a unique window into the small-scale structure of the deep Earth. We study lower mantle scattering by analyzing 412 high-quality *PKP* precursor records at ranges between 120° and 137.5° as obtained from the global seismic networks during the last 10 years. To examine regional variations in scattering strength, we compare individual records with the globally averaged *PKP* precursor stack of *Hedlin et al.* [1997]. We identify strong differences in apparent scattering strength among specific source-receiver paths. Inversion of these data for scattering source regions is complicated by ambiguity between source- and receiver-side scattering and the sparse and uneven data coverage. Synthetic tests, however, suggest that inversions with applied smoothness constraints can resolve large-scale differences in scattering strength over significant parts of the lower mantle. We use a conjugate gradient method based on an approximation to Rayleigh-Born scattering theory to image differences in the average strength of scattering within the lowermost 1000 km of the mantle. Our results indicate particularly strong scattering beneath central Africa, parts of North America, and just north of India, whereas weaker scattering is seen beneath South and Central America, eastern Europe, and Indonesia. Some regions of strong scattering correlate roughly with large-scale anomalies revealed by seismic tomography including the African plume and the Tethys trench. These correlations are tentative rather than definitive because bootstrap resampling tests show that many details in our model are not reliably resolved and the network data alone do not permit complete resolution of the source-receiver ambiguity in all areas. Further progress in this area will require integration of available network recordings with data collected by regional networks and arrays and consideration of the phase velocity of the precursors as well as their temporal variations.

1. Introduction

Earth's deep inner structure has long been the subject of intense scrutiny by seismologists and other researchers, and Earth's average radial seismic velocity structure was largely determined over 50 years ago. Large-scale seismic velocity anomalies in the mantle were identified more recently when seismologists began applying three-dimensional inversion techniques to increasing quantities of data from the global seismic networks. Intermediate-scale structures, such as descending crustal slabs or ascending mantle plumes that are believed to be associated with mantle convection, lie at or beyond the limit of resolution of existing geophysical imaging tools and are more poorly understood. Resolving small-scale structure in the deep Earth is even more challenging because of problems of spatial aliasing and the contaminating effect of strong velocity heterogeneity in the crust and upper mantle on seismic signals.

Recent advances in the quality and quantity of teleseismic data and improved analysis techniques have provided us with more detailed images of Earth's interior. Recent global tomographic images [e.g., *Grand,* 1994; *van der Hilst et al.,* 1997] have revealed continuous, high-velocity trends in the midmantle that correlate with known subduction zones, such as the Tethys and Aegean trends in southern Eurasia and the Farralon trend in central America, thus apparently imaging the continued subduction of slabs below the 660 km discontinuity. Beneath midmantle depths, however, the Eurasian trends become discontinuous, and the question of whether the slabs remain intact and continue to subduct into the deepest mantle in these areas remains open for debate [see, e.g., *Bijwaard et al.,* 1998].

Paper number 2000JB900019.
0148-0227/00/2000JB900019$09.00

For some time it has been known that small-scale heterogeneity with scale lengths of 5 to 10 km must be present at or near the core-mantle boundary to explain scattered seismic arrivals observed as high-frequency precursors to the core phase *PKP* [*Haddon*, 1972]. More recent results [*Hedlin et al.*, 1997; *Shearer et al.*, 1998; *Cormier*, 1999] have shown that this small-scale heterogeneity must extend at least 1000 km up into the lower mantle to explain the time dependence of the precursor amplitudes. Mantle heterogeneity of this scale is too small to be sustained for any length of time as thermal anomalies, implying a compositional origin [*Hedlin et al.*, 1997; *Shearer et al.*, 1998] and supporting "plum pudding" models of incompletely mixed mantle [e.g., *Davies*, 1984, 1990; *Gurnis and Davies*, 1986; *Christensen and Hofmann*, 1994; *Schmalzl et al.*, 1996]. Recently, several groups have proposed that compositional heterogeneity at a variety of scales from hundreds to several thousand kilometers may be present in the lower mantle [e.g., *Kellogg et al.*, 1999; *van der Hilst and Karason*, 1999; *Kaneshima and Helffrich*, 1999] with important implications for mantle convection processes.

Here we analyze a global data set of *PKP* precursors to identify regions within the lower mantle where high-frequency scattering is either stronger or weaker than average. Strong variations in scattering intensity are often observed for relatively small changes in ray path geometry. We invert the data for a model of average scattering strength in the lower 1000 km of the mantle using a conjugate gradient inversion method with applied smoothness constraints. Despite limitations in the available ray path coverage and ambiguities between source- and receiver-side scattering, we are able to produce a map of average scattering intensity for some regions.

2. *PKP* Precursors

Precursors to *PKP* were first observed by *Gutenberg and Richter* [1934]. The precursors precede *PKP* by as much as 18 s and increase gradually in amplitude with time and range between 118° and 145° (Figure 1). The discovery of these arrivals led to numerous early hypotheses about their origin. *Gutenberg* [1957] argued the precursors were due to refraction in the inner core. *Bullen and Burke-Gaffney* [1958] suggested that the precursors were due to diffraction of *PKP* from the core-mantle-boundary (CMB). *Bolt* [1962] and *Sacks and Saa* [1969] concluded the precursors are due to refraction or reflection of *PKP* at transition layers between the inner and outer cores. However, it is now widely accepted that *PKP* precursors are caused not by radial structures but result from scattering off small-scale topography at the CMB and/or volumetric heterogeneity in the lower mantle. The scattering diverts energy between the mantle phase *P* and the outer-core branches *PKPab* and *PKPbc* (Figure 2). The energy precedes *PKPdf*, the branch that refracts through the inner core. This explanation was first proposed by *Haddon* [1972], was presented in more detail by *Cleary and Haddon* [1972], and has been supported by numerous analyses of array recordings [e.g., *Doornbos* and *Husebye*, 1972; *King et al.*, 1974; *Husebye et al.*, 1976; *Doornbos*, 1976]. The array analyses showed that the travel times, amplitudes, slownesses, and frequency content of the precursors were consistent with the scattering theory. A scattering origin for *PKP* precursors was somewhat surprising because usually scattered waves (e.g., *Pdiff*, the coda to the compressional phase that diffracts off the outer core [*Bataille and Lund*, 1996]) arrive after the

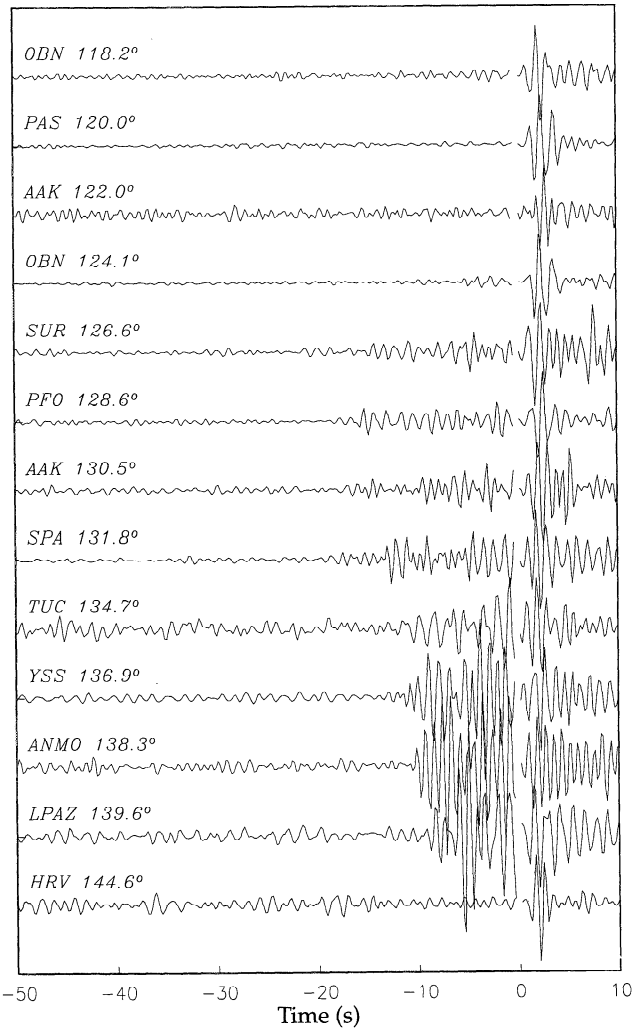

Figure 1. Examples of *PKP* precursors seen in records from stations of the Incorporated Research Institutions for Seismology (IRIS) Global Seismographic Network (GSN) between 118° and 145°. These traces have been band-pass-filtered between 0.7 and 2.5 Hz and are aligned on the *PKPdf* onset. The events occurred between 53 and 596 km in depth and had body wave magnitudes from 5.7 to 6.6. The precursors and preceding noise (at negative times) have been amplified by a factor of 7 for visual clarity. The precursors become visible near 124° and become more energetic with increasing range before disappearing at 145°. The earliest precursors arrive ~18 s ahead of *PKP*.

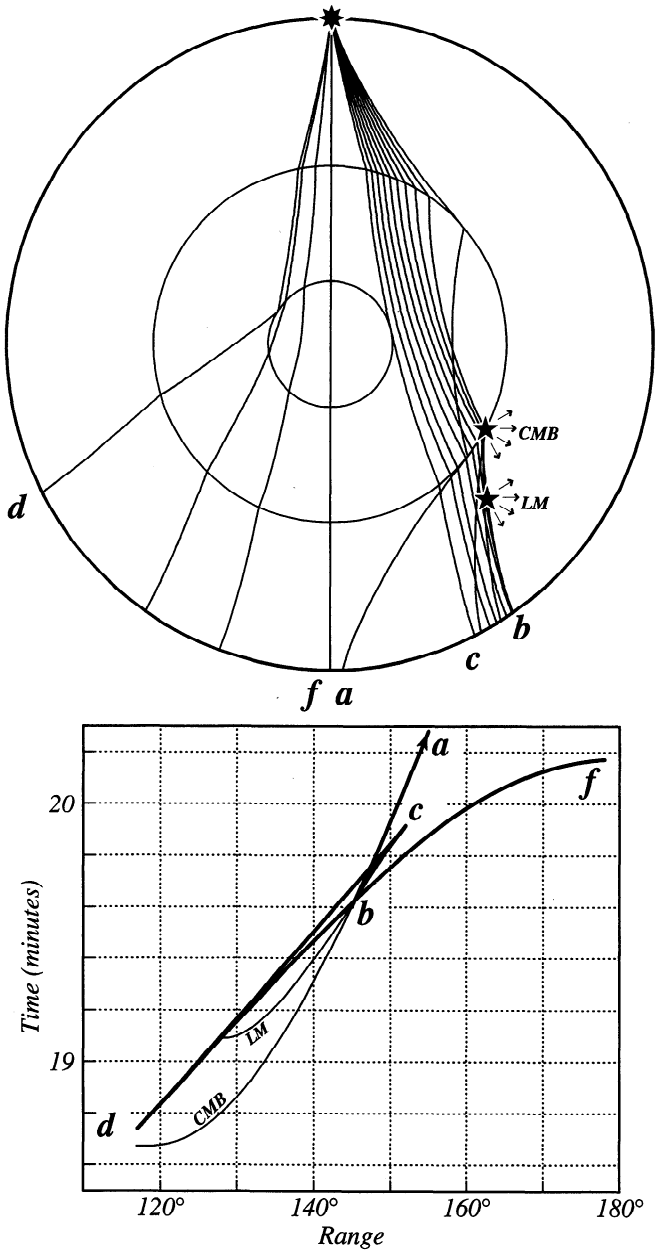

Figure 2. Ray paths and travel times of the different branches of *PKP* for a source at the surface. The retrograde *ab* and prograde *bc* branches refract through the outer core. The *cd* branch is reflected from the inner core boundary. The *df* branch refracts through the inner core. Scattering involving the *ab* or *bc* branch can produce precursory arrivals. The inner core branch *PKPdf* serves as a reference phase and is not involved in the scattering. Two hypothetical scatterers, labeled CMB (core-mantle-boundary) and LM (lower-mantle), produce precursors that can arrive no earlier than the labeled curves in the lower plot. The deepest scatterers will give rise to the earliest precursors. Although we have depicted scattering from *PKP* to *P* near the receiver, precursors can also result from scattering from *P* to *PKP* on the source side.

main phase since the total path length of a scattered phase is typically longer than that of the main arrival. *Haddon* [1972] demonstrated that *PKP* precursors are able to precede the reference phase because of the unusual ray geometries that result from the sharp *P* wave velocity drop at the CMB. Although the precursors precede *PKPdf*, this phase plays no role in their origin other than to provide a reference time. Because they arrive before any other seismic phases, *PKP* precursors provide a unique window into deep Earth scattering, as they are uncontaminated by direct arrivals and near-surface crustal scattering and resonances.

PKP precursors can result from scattering in a small volume of the lowermost mantle offset only slightly from the source and receiver locations (Figure 3). Although using arrival time alone it is not possible to unambiguously associate any precursory arrival with a specific point in the mantle or at the CMB, the ambiguity is reduced for early arrivals. Precursors that arrive at the minimum travel time (for example, on the first curve shown in Figure 2) must be due to scattering at the CMB directly beneath the source or receiver at the intersection of the *b* caustic surface with the CMB. Later arrivals can result from scattering on progressively larger surfaces that extend off the great circle path and up into the mantle (Figure 3).

Following the pioneering work of Haddon and Cleary, numerous analyses of *PKP* precursors have focused on the physical nature and the location of scatterers at the CMB and in the mantle. *Doornbos and Vlaar* [1973] and *Doornbos* [1976] concluded the scattering region extends at least 600 to 900 km above the CMB. Other studies placed the heterogeneity within the D″ layer just above the CMB [*Haddon and Cleary*, 1974] or as small-scale topography on the CMB [*Doornbos*, 1978]. *Hedlin et al.* [1997] used a stack of globally distributed Incorporated Research Institutions for Seismology (IRIS) Global Seismographic Network (GSN) recordings of *PKP* precursors to estimate the globally average precursor amplitude as a function of time and range between 120° and 145° and found that the data cannot be adequately fit if scattering is confined to the vicinity of the core-mantle boundary. They argued that significant scattering must extend at least 1000 km up into the mantle, a conclusion recently supported by the analysis of *Cormier* [1999]. Most modeling of *PKP* precursors has used ray theory and assumed single scattering (the Born approximation); a more sophisticated analysis by *Cormier* [1995] supports the validity of this approach.

Previous *PKP* precursor modeling efforts have generally focused on the depth dependence of globally averaged scattering strength. However, *Bataille and Flatté* [1988] and *Hedlin et al.* [1995] noted differences in precursor amplitude suggestive of lateral variations in the scattering strength. *Vidale and Hedlin* [1998] found evidence for intense scattering at the CMB beneath Tonga and inferred the presence of partial melt. These observations suggest that it may be possible to map large-scale variations in the strength of small-scale scattering in the lower mantle. Here we systematically examine differences between individual *PKP* precursors and their global average and invert these observations for a

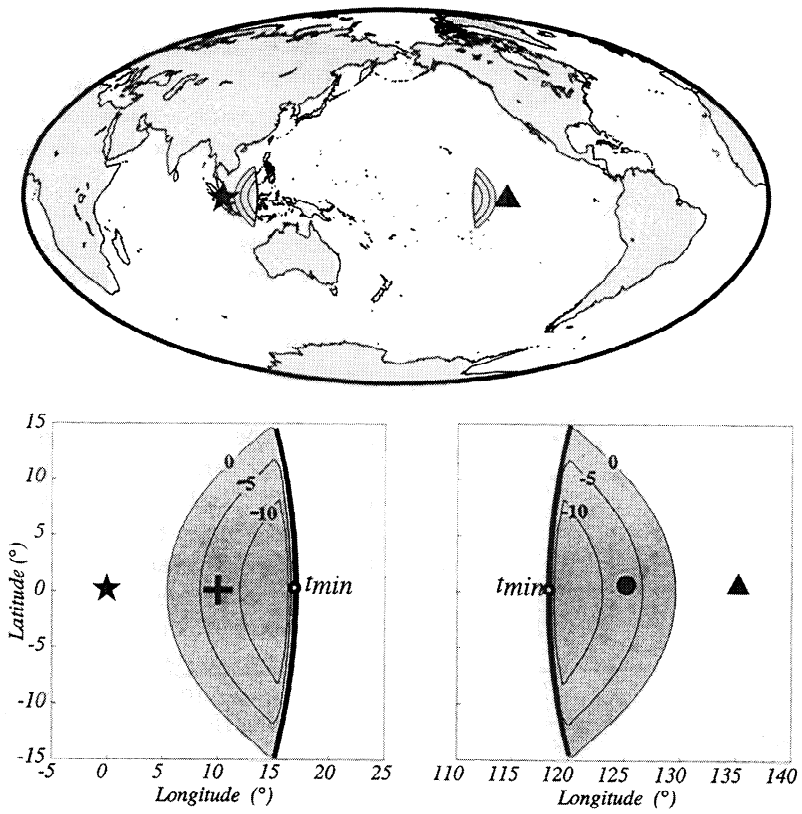

Figure 3. Precursors to *PKP* are due to scattering from a small volume of the mantle near the source or the receiver. A hypothetical source-receiver pair separated by 135° is shown above. The five-pointed star marks the source; the triangle marks the receiver. The points at which *PKPdf* enters and exits the core are marked by the cross and the circle, respectively, and are enveloped by the patches at the CMB that can give rise to precursors. The labeled curves indicate the relative advancement in seconds of the scattered phase in front of the *PKP* onset. The first arriving precursors result from scattering at the two points denoted "tmin" located on the *b* caustic. The curves labeled "0" indicate the locations at which single-scattered energy will arrive at the same time as *PKPdf*. Scattering at the CMB outside these patches will produce *PKP* coda. The area within which scattering can produce precursors becomes progressively smaller with decreasing depth. Figure 3 illustrates the degree to which lower mantle coverage is guided by the distribution of sources and receivers.

map of relative scattering intensity in the lower mantle. This work presents a more complete description of global variations in small-scale scattering strength in the mantle than has been previously published as it uses a global distribution of network recordings.

3. Globally Averaged *PKP* Precursors

To map regional variations in the strength of small-scale scattering in the mantle, we compare individual *PKP* precursor amplitudes to those of a reference image of average *PKP* precursor amplitude as a function of time and range. For our global reference, we use a stack of 1600 *PKP* recordings (as previously described by *Hedlin et al.* [1997], and *Shearer et al.* [1998]). The data are broadband records from the IRIS GSN. To avoid bias toward high-amplitude precursors, records were selected (using an automatic method for initial screening and a manual method for subsequent analysis) on the basis of low noise levels and impulsive *PKP* arrivals, regardless of whether precursors are actually visible. To estimate the average precursor amplitude, we grouped and stacked traces in 1° range bins from 120° to 145°, without regard to source or receiver location, after band-pass filtering each trace between 0.7 and 2.5 Hz, converting each to an envelope, and adjusting the amplitude slightly downward to compensate for noise. The stack, shown in Plate 1, shows a gradual but clear increase in amplitude with increasing time and range. The amplitude changes are due to several factors. The scattering volume increases with increasing time (Figure 3). The scattering angle decreases with increasing range; small-scale scattering is directional with the strongest energy being associated with the smallest scattering angle. Scattered wave strength is also strongly influenced by proximity to the *b* caustic which lies at 145°.

Hedlin et al. [1997] considered these factors and modeled this stack using Rayleigh-Born scattering theory [*Chernov*, 1960] applied to the exponential autocorre-

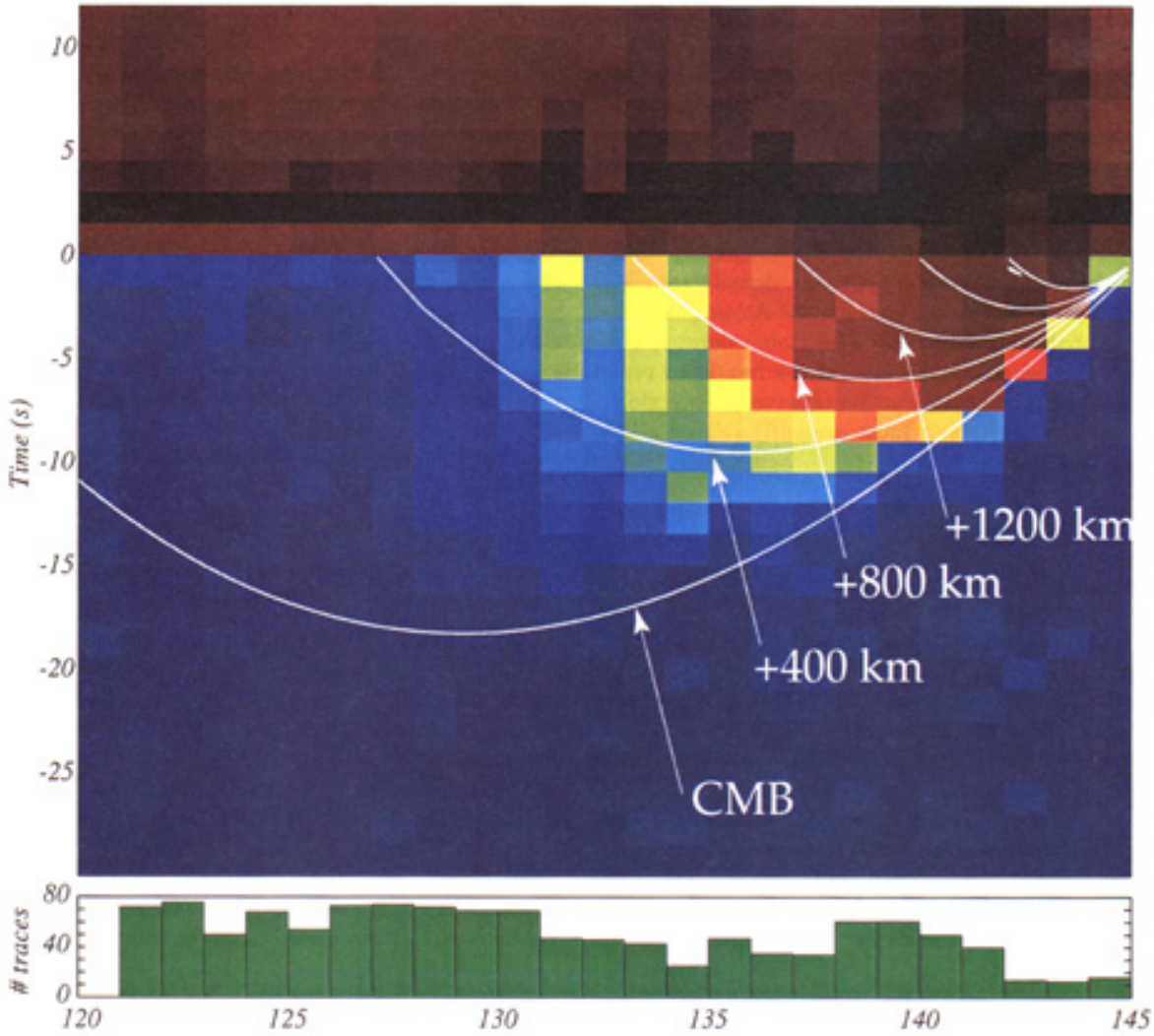

Plate 1. Average amplitude of *PKPdf* and its precursors and coda at ranges between 120° and 145°, resulting from a stack of 1600 short-period seismograms. Time is relative to the onset of *PKPdf*. The amplitude of the precursors increases gradually with increasing range and time. The precursors first appear at 124° and become indistinguishable from *PKPdf* by 143°. The white curves show the minimum travel times for scattered waves at several depths in the mantle calculated using the preliminary reference Earth model (PREM) velocity model [*Dziewonski and Anderson*, 1981]. Scattering that occurs at the CMB gives rise to the earliest precursors. Scattering in the outer core can produce earlier arrivals, but none are observed. The increase of coda amplitudes with increasing range seen in Figure 1 is evident here. The bottom plot shows the number of traces used in each 1° bin. Relatively few traces were selected beyond 142° because of the inherent difficulty in separating *PKP* from its energetic precursors.

lation fuction and concluded that the global average small-scale heterogeneity has a scale length of ~8 km with an rms velocity contrast of 1%. The adherence of the onset of precursors with the minimum travel time for scattering at the CMB (Plate 1) precludes scattering within the outer core which would produce arrivals before the observed onset of the precursors [*Shearer et al.*, 1998].

Because the scattering volume tracks the *PKPdf* core entry and exit points, global coverage is well summarized by the points in Figure 4. In Figure 4 we plot sources, receivers, and *PKPdf* core entry and exit points and see that even a relatively uniform global network such as the IRIS GSN offers highly variable coverage. Some areas, such as those near the seismically active regions in the southwest Pacific, are densely sampled, while other regions (e.g., beneath the Atlantic and Indian oceans) are untouched. The global network coverage is limited largely because of the restricted range within which precursors can be observed. Any global study of *PKP* precursors must presently rely on a limited sampling of the mantle.

4. Some Anomalous Recordings

Any scattering theory that assumes globally uniform heterogeneity will predict a steady increase in precursor amplitude with range and would not explain the small-scale structure evident in the stack shown in Plate 1. For example, the bin from 132° to 133° has notably less energy than the neighboring bins. The events in this bin are not from a single region but are distributed broadly across the southwest Pacific and western South America. Most stations that recorded these events were located in Eurasia and North America. This structure hints at complex regional variations in the strength of scattering in the mantle; chacterizing and mapping these variations is the primary focus of this paper. An example of this variability is given in Figure 5, comparing records from two different deep events in the southwest Pacific as recorded by IRIS GSN station DBIC in Ivory Coast. The recording of the northern event was made at 134.3° and is shown in the upper part of the bottom plot. At this range, energetic precursors are predicted by the global stack and its best fitting model (dashed curve), but the observations show no precursors even with the low noise levels on the record. The southern event was recorded at a range of 124.9° where our model predicts essentially no precursors, but the data show extremely energetic precursors. As shown in Plate 1, at this distance the scattering that gives rise to the precursors must occur within 400 km of the CMB. Although these records argue for significant lateral variations in scattering strength within D″, it is not possible to resolve these variations with only two records, particularly given the source-receiver ambiguity in scattering source regions. To obtain a more complete picture of scattering variability, it is necessary to examine many different ray geometries.

Of the 1600 recordings in the global stack, we selected 412 higher-quality records for further analysis, basing our selection largely on the level of noise preceding the precursor wave train. In the global stack most bins contain over 40 recordings, and so inferior traces are averaged out. In the mapping we are about to describe, the redundancy of coverage is much lower as recordings are not binned by range but by the volume of the mantle sampled, and a few noisy traces can lead to large artifacts in an inversion. Examples of the best traces are summarized in Figure 6. All plots in Figure 6 show the ratio of average precursory energy in each trace to that predicted as a function of range. These energy ratios clearly have a lognormal distribution about the global average. When we examine traces from particular source regions or stations, some consistent anomalies are observed. Recordings made by the station in Al-

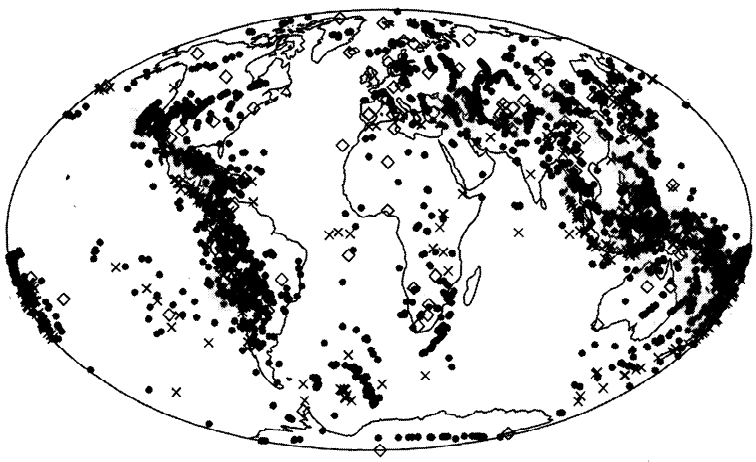

Figure 4. Map showing the *PKPdf* entry and exit points on the CMB for the 1600 seismograms in the stack of *PKP* precursors shown in Plate 1. Source locations are shown as crosses; receiver locations are shown as diamonds.

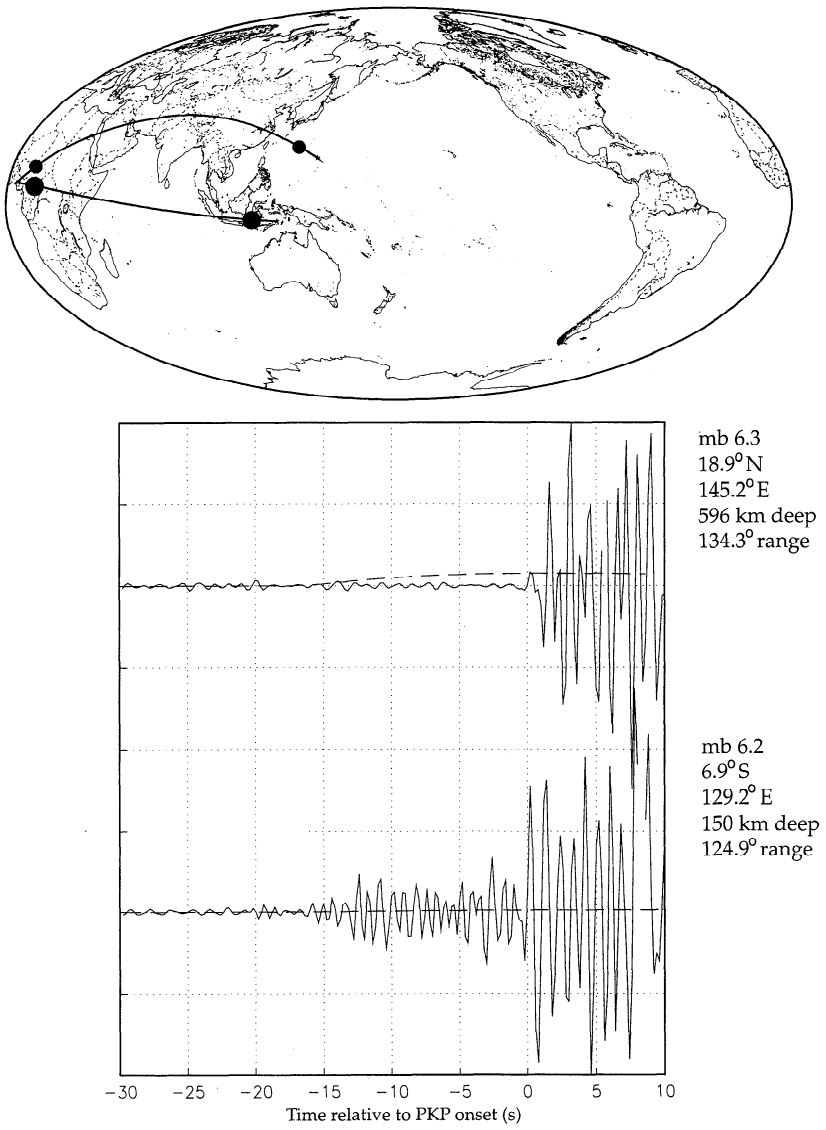

Figure 5. Data from the IRIS-GSN station DBIC in Ivory Coast give an illustration of the dependence of precursor strength on ray path. Two events are plotted. The first, shown in the top trace, occurred near Guam at a range of 134.3° where energetic precursors are normally detected. The observed precursors are obscured by noise and are much less energetic than the global average (denoted by the dashed curve). The second event occurred south of Indonesia and was recorded by DBIC at 124.9° (second trace). This event produced significantly more precursory energy than expected.

ibek, Turkmenistan, and by stations in North America are consistently above the global average. Recordings made by the station near Arti, Russia, and near the Chinese station XAN are typically substantially below the global average. Other stations, such as DBIC in Ivory Coast and SDV in Venezuela give mixed results. As seen in Figure 5, markedly different precursor amplitudes can be observed at the same station.

A second illustration of this variability is given in Figure 7. Two record sections are included, one with recordings made by ABKT in Turkmenistan and the other made by ARU, a station near Arti, Russia. Although the two stations are separated by only 18.5°, the precursors they record are markedly dissimilar. From 126° to 137°, ABKT records much more energetic *PKP* precursors than ARU. Most of these events are located in the southwest Pacific, suggesting that strong variations in the strength of scattering exist beneath central Asia.

To show the full global distribution of our data and identify those paths with anomalous *PKP* precursor amplitudes, in Figure 8 we plot the *PKPdf* entry and exit points with symbols that are scaled by the full-trace energy ratio. This exercise is intended to illustrate some large-scale trends and does nothing to deal with the entry-exit ambiguity. For each trace a symbol is lo-

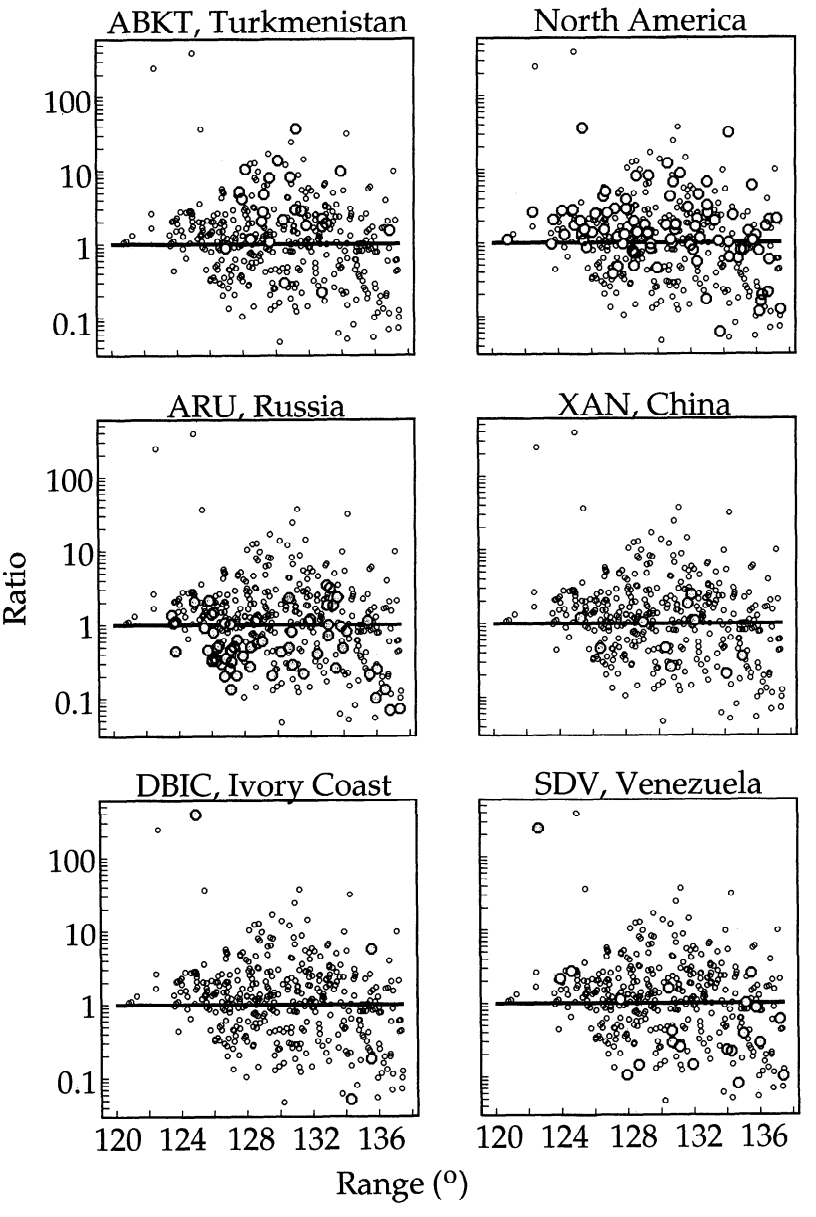

Figure 6. The deviation of observed precursor amplitudes from the global average is not random but has a strong dependence on location. In each plot, we show the ratio of the energy observed in recordings made at selected stations to that predicted by the global model of *Hedlin et al.* [1997] which has 1% rms velocity perturbations throughout the mantle. These energy ratios, plotted as a function of source-receiver range, are represented by the large shaded symbols. In all plots, the small open circles denote energy ratios from all 412 events used in this study. Energy ratios from the full data set are lognormally distributed about 1. As seen in the upper left plot, recordings made by the GSN station in Turkmenistan are consistantly above the average. The North American recordings (made by CMB, PAS, DGR, GSC, BAR, PFO, GLA, TUC, ANMO, FFC, CCM, SSPA, HRV, and ALE) are also consistently above the global average. The station near Arti, Russia, and the station XAN in China typically record weak precursors. Other stations produce mixed observations. The amplitude ratios from two DBIC recordings shown in Figure 4 are displayed in the bottom left plot here.

cated at the points at which *PKPdf* enters and exits the core. The top and bottom illustrations show the traces that are above and below the global average, respectively. Some regional trends are clearly indicated, such as strong scattering beneath central Africa and weak scattering beneath Eurasia. Mixed results in many regions underscore the need for reducing the entry-exit ambiguity.

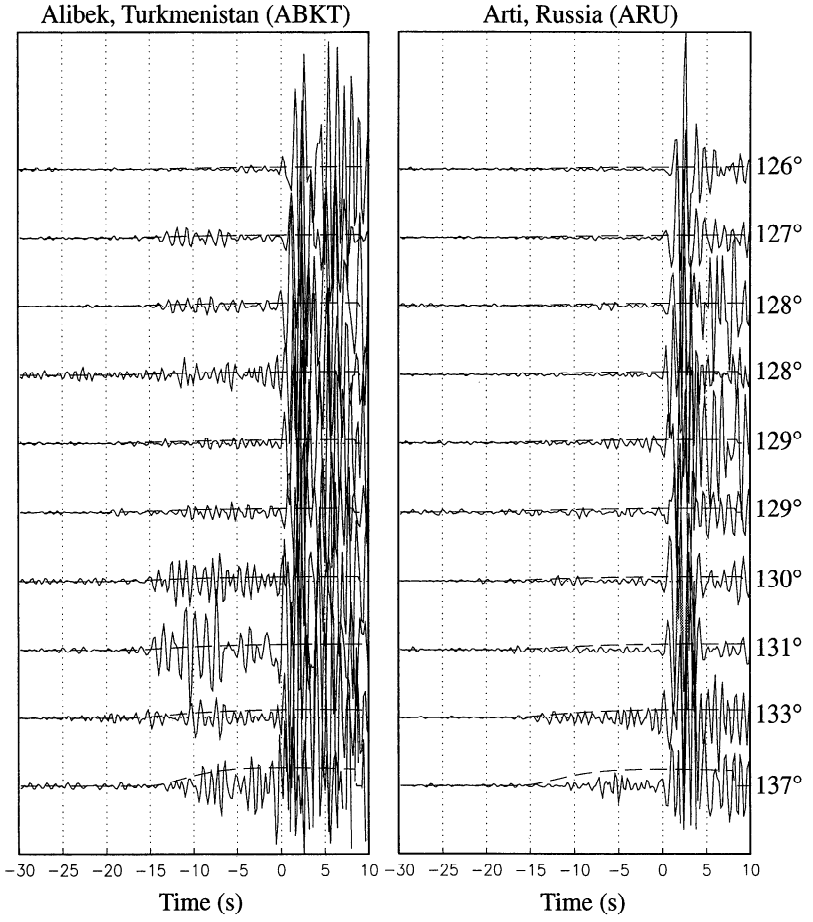

Figure 7. The GSN stations in Turkmenistan and near Arti, Russia, are separated by just 18.5° but record markedly dissimilar precursors. These record sections illustrate that ABKT consistently records precursors that are above the global average (shown at each range by the dashed curve), while most precursors recorded at ARU are less energetic than the global average.

5. Inversion of *PKP* Precursors for a Scattering Model

If the heterogeneity in the mantle and at the CMB were statistically invariant, the resulting high-frequency precursors to *PKP* would still show variations with time and with range. Precursors resulting from such an Earth would grow in amplitude gradually and continuously from onset until after the arrival of *PKP*. This is largely because late arrivals can come from a progressively larger volume that reaches into the shallow mantle and off the great circle path between the source and receiver. Owing to a number of factors, including scattering angle, scattering volume, and proximity to the *b* caustic, *PKP* precursors are strongly dependent on range. The precursors grow in amplitude continuously along the *df* branch of *PKP* from the first observations near 120° to the *b* caustic. This time and range dependence was modeled by *Hedlin et al.* [1997] using Rayleigh-Born acoustic scattering theory [*Chernov*, 1960] adapted for an elastic medium [*Haddon and Cleary*, 1974]. Assuming single scattering in a Poisson solid with an exponential autocorrelation function [*Wu and Aki*, 1985] the average scattered power is given by

$$< |\Phi_s(\theta)|^2 > = \frac{2k^4 a^3 \tilde{\alpha}^2 V A^2}{\pi r^2} \frac{\frac{1}{4}\left(\cos\theta + \frac{1}{3} + \frac{2}{3}\cos^2\theta\right)^2}{\left(1 + 4k^2a^2\sin^2\frac{\theta}{2}\right)^2}, \quad (1)$$

where θ is the scattering angle, A is the incident wave amplitude, V is the volume of scattering, $\tilde{\alpha}$ is the rms velocity perturbation $(\delta\alpha/\alpha_0)$, a is the characteristic scale length, k is the wavenumber(ω/α_0), and r is the scatterer-to-receiver distance. The $1/r^2$ factor, applicable in a simple whole space, must be replaced with the appropriate geometric spreading factors determined by ray tracing and CMB transmission coefficients for propagation into and out of the core. The scattering angle is the angle by which the energy is diverted from its original path and may also be estimated by ray tracing.

The gradual and continuous increase in observed precursor amplitude with time (see Plate 1) argues against an upper depth limit to small-scale heterogeneity in the mantle, at least within approximately the lower-

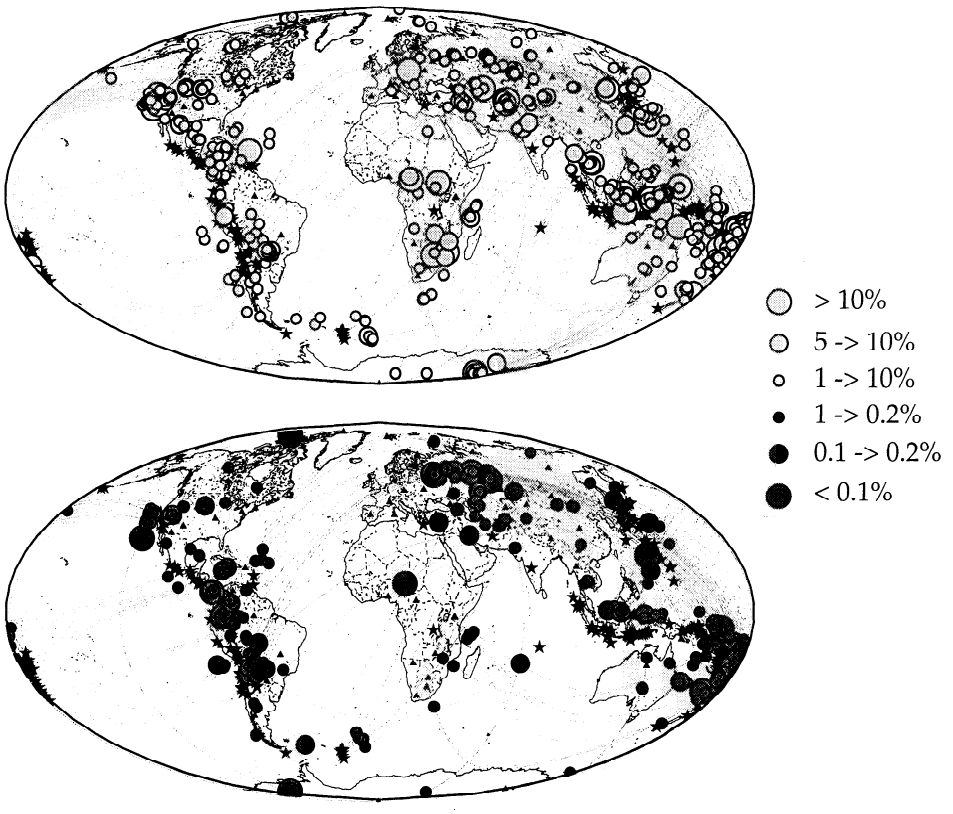

Figure 8. The traces from the full data set that are found to be consistent with scattering that is stronger than the global average are shown in the top illustration. All other traces are shown in the bottom illustration. In both illustrations, the symbols scale with rms velocity perturbation with the largest symbols representing the greatest deviation from the global norm. Each trace is associated with two symbols, one at the source end and another near the receiver. The curves are the great circle paths between source and receiver.

most 1000 km [*Hedlin et al.*, 1997; *Shearer et al.*, 1998; *Cormier*, 1999]. *Hedlin et al.* [1997] found that the best fit to the stacked precursors was given by a model that has random heterogeneity of ~1% rms velocity perturbation and an ~8-km scale length throughout the mantle.

The primary goal of the current work is to associate anomalous precursor recordings (such as those displayed in Figures 5 and 7) to excursions of the small-scale heterogeneous velocity structure of the mantle from the global average. To do so requires that we take into account that a precursor at any time and range can result from scattering in an extended volume. The uncertainty as to the point of scattering is minimal for points at the precursor onset (Figure 3). This energy is due to scattering at the CMB beneath the source and/or receiver. Progressively more ambiguity, however, is associated with later arrivals. Rayleigh-Born theory may be used to define the forward problem, given a linear relationship between any single data point and scattering strength throughout the appropriate volume. If a reference Earth model is assumed and the heterogeneity scale length is held fixed, then the relationship between the entire set of recordings and the scattering strength in the mantle may be expressed simply as

$$\mathbf{d} = \mathbf{G}\mathbf{m}, \tag{2}$$

where $\mathbf{d}$ is the data vector which consists of a concatenation of all individual recordings (converted to power), $\mathbf{G}$ is the matrix which describes the linear relationship between the data vector and the model vector $\mathbf{m}$, which is a measure of the scattering strength $\tilde{\alpha}^2$ within a series of specified volume elements. The elements of $\mathbf{G}$ are given by (1), as simple ray tracing provides the scattering angles θ, the geometrical spreading terms, etc., for each point in the model.

Note that (1) and (2) do not relate specific velocity perturbations in a model to individual wiggles on the seismograms; rather they describe the statistical relationship between random heterogeneity within a volume and the average power of the scattered waves. Inversion of (2) is complicated by the fact that both $\mathbf{d}$ and $\mathbf{m}$ contain only positive values. To develop an approximate solution to (2), we consider perturbations of $\mathbf{d}$ and $\mathbf{m}$ about reference values $\mathbf{d}_0$ and $\mathbf{m}_0$, that is

$$\mathbf{d}_e + \mathbf{d}_0 = \mathbf{G}[\mathbf{m}_e + \mathbf{m}_0], \tag{3}$$

where $\mathbf{d}_e = \mathbf{d} - \mathbf{d}_0$ and $\mathbf{m}_e = \mathbf{m} - \mathbf{m}_0$. We obtain $\mathbf{m}_0$ and $\mathbf{d}_0$ from our best fitting globally averaged model and its predicted precursor power levels. Thus, by definition, $\mathbf{d}_0 = \mathbf{G}\mathbf{m}_0$ and

$$\mathbf{d}_e = \mathbf{G}\mathbf{m}_e. \tag{4}$$

For $|\mathbf{d}_e| \ll \mathbf{d}_0$ and $|\mathbf{m}_e| \ll \mathbf{m}_0$, we have the approximations $\mathbf{d} - \mathbf{d}_0 \approx \mathbf{d}_0 \log(\mathbf{d}/\mathbf{d}_0)$ and $\mathbf{m} - \mathbf{m}_0 \approx \mathbf{m}_0 \log(\mathbf{m}/\mathbf{m}_0)$, and thus we may write

$$\mathbf{d}' = \mathbf{G}\mathbf{m}', \tag{5}$$

where $\mathbf{d}' = \mathbf{d}_0 \log(\mathbf{d}/\mathbf{d}_0)$ and $\mathbf{m}' = \mathbf{m}_0 \log(\mathbf{m}/\mathbf{m}_0)$. Although it is only an approximation to (2), this equation has the advantage of allowing both positive and negative values for data and model as well as accounting for the fact that scatter in the data seems lognormally distributed.

Our goal is to invert this equation for a laterally varying model. This problem has some similarities to reflection seismic analyses used by the oil industry to image subsurface reflectors. The goal in both cases is to identify the scattering source regions given data from surface sources and receivers and assuming a reference velocity model. It is common practice in seismic reflection processing to invert equations such as (2) or (5) using simple stacking and backprojection techniques. This is unlikely to be effective for our problem because of the sparse and uneven coverage of our data and the source-receiver ambiguity in the source regions. Thus we attempt a more complete inversion of (5) to better address these difficulties. Such an inversion, while computationally intensive, is made practical by the relatively small number of data we have available (412 seismograms).

We define a grid of model points spaced every 2° in latitude and longitude and 50 km in depth from the CMB to 1000 km above. Each of the 21 layers of the model thus has 16,471 points. To make the calculation tractable, we average each column of model points to a single value and thus compute an image that represents the average scattering strength in the lowest 1000 km of the mantle. Although we ultimately only solve for a one-layer model, we use the 50-km layer spacing to take into account the depth dependence of the kernels in the $\mathbf{G}$ matrix. As seen in Figure 2, the earliest arrivals result from scattering at the CMB, and so coverage is dominated by the deepest layers in the mantle.

For a given source-receiver geometry and model point a travel time may be computed for the source-to-scatterer-to-receiver ray path. If this time is before the corresponding time of *PKPdf*, then a contribution to the precursors is possible and the time may be associated with a single point on the appropriate seismogram. We process our data by squaring the envelope function to obtain a measure of power versus time. To properly model the data, it is necessary to assume a realistic source-time function. We derive an empirical source-time function using a stack of the direct *PKPdf* arrivals and convolve this function (in power) with our model predictions. The use of a source-time function in this way greatly increases the number of nonzero elements of $\mathbf{G}$. A sparser $\mathbf{G}$ matrix would be possible if the source-time function were deconvolved from the data prior to analysis, but we preferred to avoid the instabilities associated with deconvolution.

Our model is severely overparameterized compared to our data constraints; thus some form of regularization is necessary to stabilize the inversion. We apply a smoothness constraint in which we minimize model roughness by inverting the following system:

$$\begin{bmatrix} \mathbf{d}' \\ 0 \end{bmatrix} = \begin{bmatrix} \mathbf{G} \\ \lambda\mathbf{L} \end{bmatrix} \mathbf{m}' \tag{6}$$

in which $\mathbf{L}$ represents a simple four point horizontal Laplacian and λ is an adjustable parameter that controls the degree of smoothing. We invert (5) using a conjugate gradient inversion technique [*Hestenes and Stiefel*, 1952].

The data coverage on the CMB provided by the reduced data set of 412 traces is plotted in Plate 2. A checkerboard test illustrates the effectiveness of our inversion method when using the existing coverage applied to perfect, noise-free data. In Plate 3 we display an input pattern which is simply the product of sinusoids dependent on latitude and longitude. We simulate data without introducing noise and assuming that $\mathbf{G}$ is exactly known. The recovered pattern results after 500 iterations from an inversion using a λ value of 24. The selection of this degree of smoothing, which is used throughout this work, is somewhat subjective as we do not have a way of predicting the expected noise level and thus do not know how well we should be able to fit the observed data. Our choice was guided by a visual inspection of the images. The number of iterations was set at 500 since additional iterations yielded no appreciable improvement in the fit. In most regions of the synthetic model the original pattern is accurately resolved. The data variance reduction for the overall pattern shown in Plate 3 is 85%. In some areas where the sampling is sparse, such as beneath the Indian Ocean, the recovery is inexact.

An inversion of the full 412 trace data set is shown in Plate 4. As in the synthetic test, the inversion employed a λ value of 24 and 500 iterations. For the real data, however, the variance reduction was only 25%. Some significant anomalies are evident in Plate 4. As expected, the inversion indicates a transition from strong to weak scattering from central to western Asia. Weak scattering is inferred to exist beneath much of South America with stronger scattering to the north. A significant high-amplitude anomaly is placed beneath Africa.

Model amplitudes shown in Plate 4 represent values of $\tilde{\alpha}^2$ in (1) and vary by factors of 0.1 to 10 from the

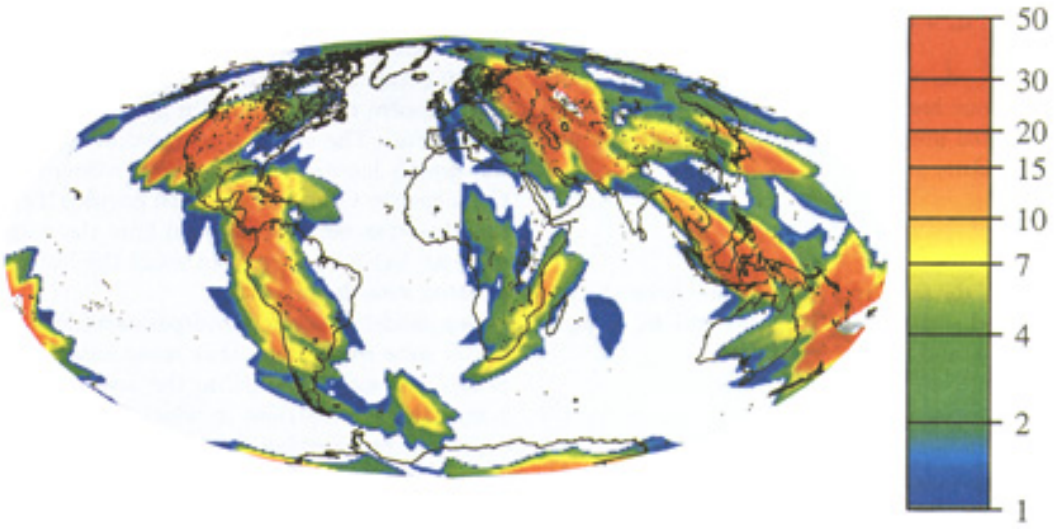

Plate 2. Data coverage as measured by the number of records which sample points on the core-mantle boundary. Coverage is largely guided by the distribution of sources and receivers and is greatest in the seismically active regions northeast of Australia and under Indonesia. Dense coverage is also provided by the stations in North America and central Eurasia. Most of the globe, however, is not sampled by *PKP* precursors.

reference model ($\tilde{\alpha} = 1\%$), corresponding to 0.3% to 3% rms velocity perturbations. However, these amplitudes are unreliable at the lower and upper limits because they violate the small-perturbation approximation used to derive (5). In fact, the precise degree of scattering in the low-scattering regions cannot be resolved and could be zero; correspondingly, the velocity perturbations in the high-scattering regions are likely less than indicated in Plate 4. Thus we caution that our inversion results should be used mainly simply to distinquish between regions of stronger and weaker scattering, without assigning precise numbers to the absolute amplitudes in the model.

To evaluate the significance and robustness of these results, we estimated standard errors using a bootstrap method [e.g., *Efron and Tibshirani*, 1991] in which we performed 100 different inversions of random selections of 412 traces from the original data set. As the selection was with replacement, some of the traces in each separate data set appear more than once; others are not selected. The mean value of the 100 bootstrap models obtained with these inversions shows no significant differences from the model obtained with the original data set. Some details of the models, however, vary greatly among the bootstrap inversions and provide insight as to which model features are robust. To show this, we mask all regions except those that lie beyond 1 standard deviation (1 SD) from the mean (Plate 4b) and beyond 2 standard deviations (2 SD) from the mean (Plate 4c). Much of the strong scattering anomaly beneath Africa is above the 1 SD limit, and a small part of this anomaly lies beyond the 2 SD limit. The transition from strong scattering north of India to much weaker scattering to the west appears to be significant. Much of the region of weak scattering beneath the Caribbean also appears in Plates 4a-4c. The strong scattering off the west coast of North America is significant at the 2 SD level. The strong scattering beneath eastern North America appears to be less robust. The bootstrap test indicates that the weak scattering north of Indonesia is significant.

A second view of image stability is given by the three separate inversions shown in Plate 5. Each inversion was taken from a single bootstrap sampling of the entire data set. The subtle details of the anomalies mentioned above are clearly not well resolved. The features beneath the southwest Pacific and Australia are highly dependent on the data sample used.

6. Discussion

6.1. Geodynamic Implications

Resolving the location and nature of scatterering source regions is important because they provide some of the best constraints on small-scale heterogeneity in the mantle. The model of *Hedlin et al.* [1997] contained uniform scattering in the lower mantle but was based on a globally averaged stack and thus could not address the question of whether the scattering is, indeed, laterally homogeneous or whether the stacking procedure has averaged out significant regional variations. Our results here strongly favor the latter possibility, but we need to determine which of these variations are significant, where they belong, and what they tell us about Earth.

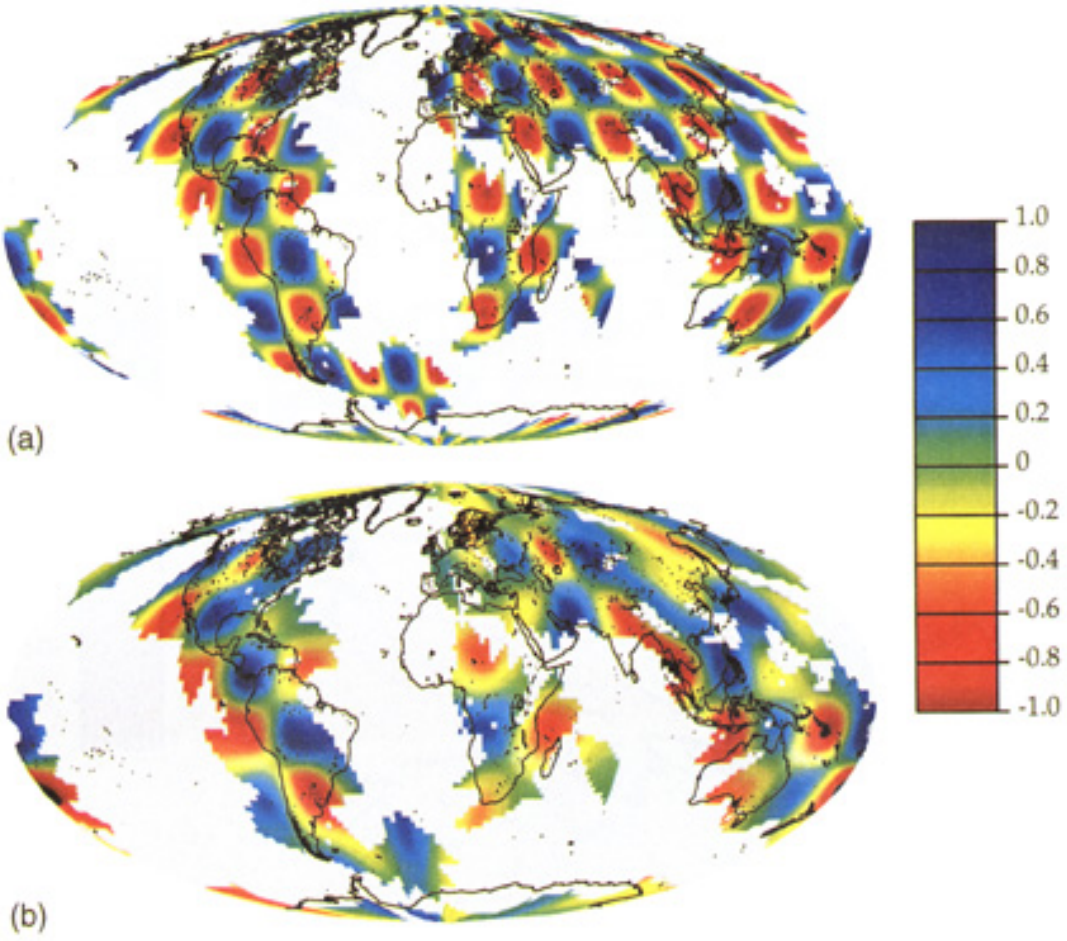

Plate 3. A conjugate gradient inversion of a checkerboard scattering pattern: (a) original pattern is the product of sinusoids dependent on latitude and longitude, and (b) recovered pattern. This image results after 500 iterations from an inversion using a λ value of 24. In this test, no noise was added to the synthetics. Both the original and recovered patterns are masked to be consistant with the recorded data. The color scale shows the logarithm (base 10) of the rms amplitude of small-scale velocity heterogeneity in the model relative to the global average. Blue indicates stronger heterogeneity and scattering; red indicates weaker heterogeneity and scattering.

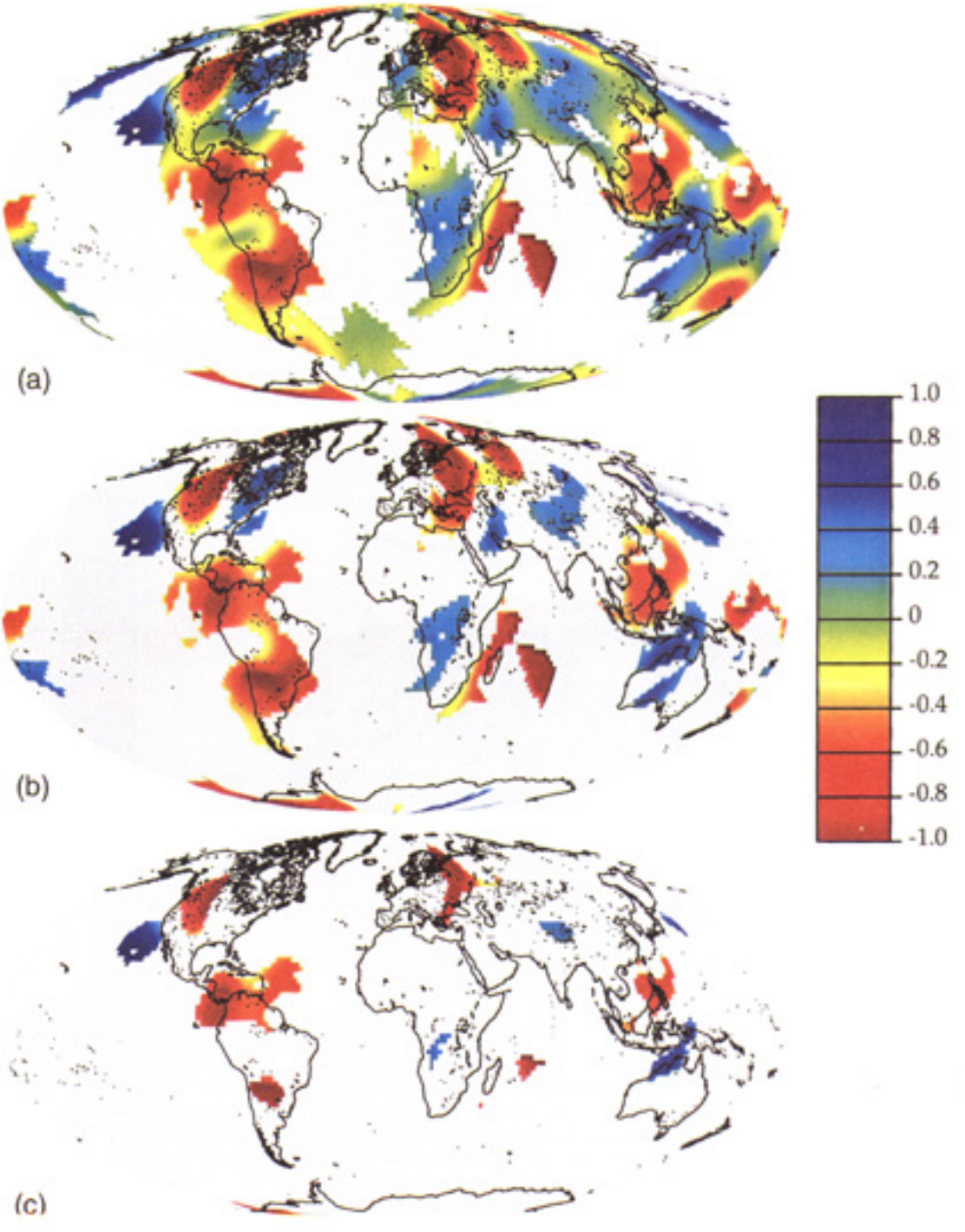

Plate 4. (a) A conjugate gradient inversion of the full data set. This image is essentially identical to a stack of 100 bootstrap inversions. (b) Masking of all unsampled regions and all regions less than 1 standard deviation away from the mean. (c) Scattering strength in regions more than 2 standard deviations from the mean. Color scale is as in Plate 3.

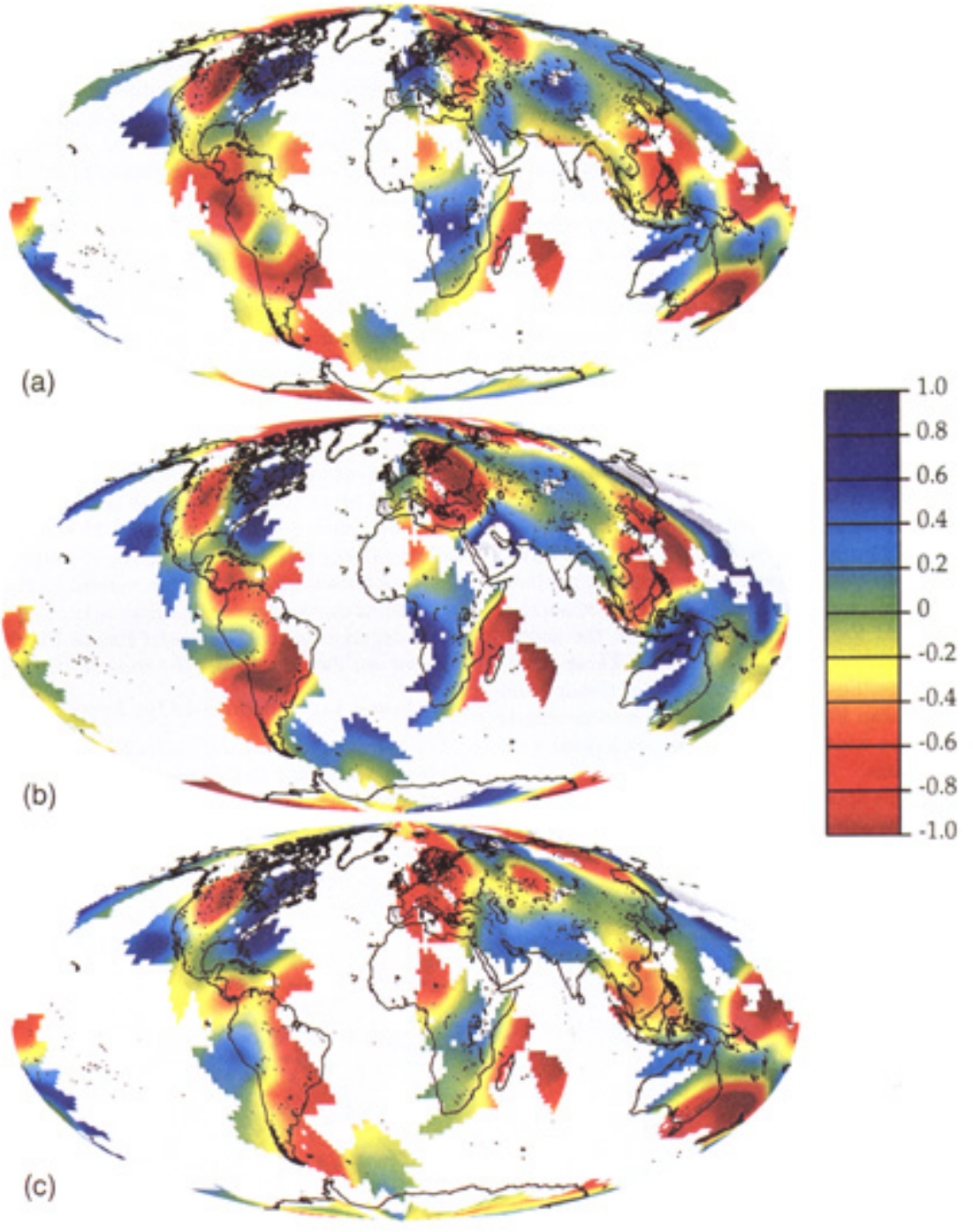

Plate 5. Conjugate gradient inversions of resampled data sets. For each image, the full data set was resampled with replacement and inverted using the same inversion parameters listed in Plate 3. Differences among these models show the unreliability of many of the small-scale features in the model; however some large-scale features, such as the African anomaly, appear to be robust. Color scale is as in Plate 3.

Intuitively, we might expect heterogeneity to become concentrated near subduction zones and upwellings, and thus regional variations in the strength of scattering might give some insights into the nature of mantle convection. The precursors we have analyzed come from the deepest 1000 km of the mantle. Within this depth interval, tomographic studies typically show strong large-scale structures in the D″ region in the lowermost mantle but show only weak anomalies (which are incoherent at large scales) at 1900 km depth in the midmantle. At more shallow depths the tomographic images of *Grand* [1994] and *van der Hilst et al.* [1997] show long continuous structures in the middle and upper mantle. Intriguingly, our scattering image exhibits little correlation to tomographic images in the lowermost mantle but does appear somewhat correlated to images of the midmantle. The *P* wave image of van der Hilst et al. shown in Plate 6 shows clearly the Tethys high-velocity trend in southern Asia and the Farralon trend cutting across North America, both of which are believed to be due to cold subducted slabs. Tomographic images of velocity at deeper levels indicate that the large-scale high-velocity trends become fragmented, and so the question of how much of the material subducted to the midmantle continues into the deepest mantle is open for debate [e.g., *van der Hilst and Karason*, 1999]. This image also shows significant low-velocity anomalies in the southwest Pacific and beneath central Africa. These structures, named the "Equatorial Pacific Plume Group" and the "Great African Plume," respectively by *Dziewonski et al.* [1991], are widely believed to be associated with mantle upwellings.

There are some apparent correlations between our image of scattering strength and the tomographic image shown in Plate 6. Some of the strongest scattering is located just north of India beneath the Tethys trend. Another location on the Tethys trend beneath Indonesia is also associated with very strong scattering. The inversion places much weaker scattering north of the Tethys trend beneath eastern Europe. Possible causes of strong scattering at the location of a subducted slab include heterogeneity in the subducted crustal material [e.g. *Gubbins and Snieder*, 1991], fragments entrained during subduction [*Christensen and Hofmann*, 1994], or fragments resulting from the breakup of the original slab. The correlations we have just noted might give evidence for deeper convection in these regions because the depth range of our image is substantially below the depth of the image shown in Plate 6.

The bootstrap analysis suggests that the strong scattering beneath central Africa is also significant. This structure is coincident with the Great African Plume of *Dziewonski et al.* [1991] and is also seen in the tomographic image shown in Plate 6. Strong scattering can be due to positive or negative velocity perturbations. In this case it seems likely that the strong scattering is a result of partial melt or small-scale (10 to 12 km) vertical plume conduits associated with the mantle upwelling [*Stacey and Loper*, 1983; *Loper* 1991]; however, this hypothesis requires a more careful analysis. No conclusions can be drawn regarding scattering strength at the location of the Equatorial Pacific Plume Group because our data cover just the flank of this region.

6.2. Some Limitations of Our Image

We currently regard the correlations between areas of strong scattering and large-scale structures revealed by other studies as tentative rather than definitive for several reasons. The network stations are sparse, and the events they record are tightly clustered along seis-

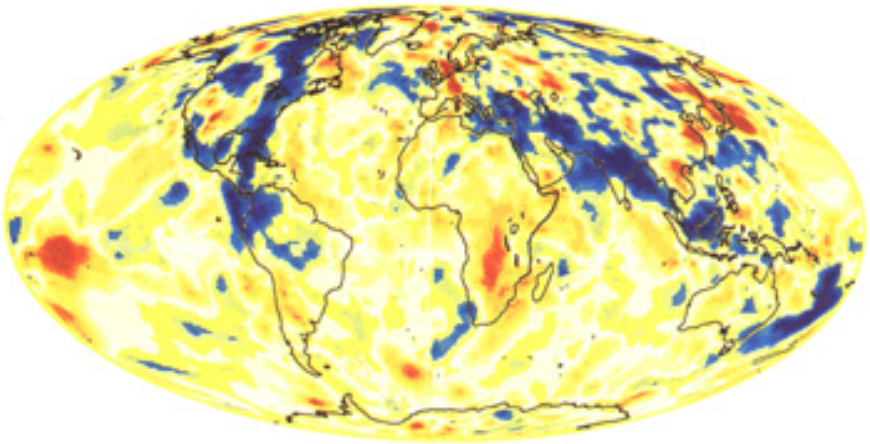

Plate 6. A tomography image of mantle *P* velocity at 1350 km depth adapted from *van der Hilst et al.* [1997]. Blue indicates fast velocity regions; red indicates slow velocity regions (with velocity perturbations given by the color bar). Note the apparent correlation between this image and some of the features in Plate 4.

mogenic zones. Sparse sampling of an uneven distribution of sources gives a data set in which crossing paths are relatively rare. One exception to this is the Tonga-Fiji trend earthquakes which are recorded by stations in central Asia, central Africa, and the Americas. Without crossing paths and without a means to accurately estimate the phase velocity, it is not possible to determine which side of the propagation path the energy came from. The energy must be allocated equally to both ends of the path. The source-receiver ambiguity is particularly problematic when an energetic precursor is recorded. When essentially no energy is recorded at a range where an average precursor has substantially more, we can place a tight constraint on mantle scattering. Such traces indicate an absence of scattering at both ends of the path; there is no ambiguity if there is no energy. For this reason we believe that the inversion provides strong evidence for weak scattering beneath Central and South America.

An undamped inversion of GSN recordings of *PKP* precursors contains much small-scale structure that defies interpretation. In part, an interpretation of this complex image is pointless because of the sparseness of the network data. Much of this fine-scale structure is aliased, and as a result we chose a highly damped inversion. From the work of *Vidale and Hedlin* [1998], *Wen and Helmberger* [1998], and others it is known that very small scale variations in the strength of scattering exist. *Vidale and Hedlin* [1998] observed extremely energetic precursors to *PKP* in NORSAR recordings of Fiji-Tonga events. The precursors sampled a small region at the CMB beneath Tonga and beneath Europe. From an array analysis of these observations they concluded the precursors stemmed from scattering at the CMB beneath the source. From a Rayleigh-Born modeling of the amplitudes they inferred partial melt in the deepest 60 km of the mantle beneath Tonga between 170° and 190° longitude and from -10° latitude to the equator. Although this area lies on the fringe of our coverage, the global network image includes a sharp increase in scattering strength at the location of the Vidale/Hedlin anomaly; however, the bootstrap analysis indicates much of the anomaly imaged by GSN data alone is not highly significant. The mismatch between the scattering strengths inferred by the GSN and by NORSAR underscores the existence of very rapid changes in the properties of the small-scale heterogeneity that lie beyond the resolution of the damped global data. Array data, such as that recorded by NORSAR, should require less damping and permit more definitive answers about the nature of fine-scale heterogeneity in the mantle at least at regional scales.

Although the bootstrap test indicates which features in the inversion are most robust, it is difficult to determine the extent to which the source-receiver ambiguity has been suppressed and thus the degree to which the energy is correctly allocated. The test shown in Plate 3 gives a highly optimistic assessment as the synthetic data are perfectly known. Figure 8 indicates that some crossing paths exist, but most sampled regions are dominated by recordings of events in a single-source region made by the same receivers. One exception is the southwest Pacific earthquake trend where recordings are made by stations in central Asia, the Americas, and Africa.

6.3. Some Comparisons With Other Studies

Other researchers have found evidence for regional variations in the strength of scattering that are consistent with our global model. From an analysis of *PKP* precursors recorded by the Yellowknife array (YKA), *Bataille and Flatté* [1988] tentatively concluded that weak scattering exists beneath central North America. Recently, *Wen et al.* [1998] found evidence for very strong scattering beneath central southern Africa with a rapid transition to weak scattering to the east.

Small structures in the deep mantle have been the subject of numerous studies using a variety of seismic phases. The area beneath Tonga identified by *Vidale and Hedlin* [1998] as being the site of strong scattering was previously identified by several authors [e.g., *Garnero and Helmberger*, 1995, 1996; *Wen and Helmberger*, 1998] as the approximate location of a 5- to 40-km-thick ultralow-velocity zone (ULVZ) at the CMB. These studies used precursors to the *SKS* phase. A comparison of our inversion with the distribution of ULVZs discussed by *Williams et al.* [1998] indicates no significant correlation between ULVZs and strong scattering in the deep mantle. Although this comparison is hampered by the limited overlap of sampling, in some areas there clearly is a lack of correlation. For example, the ULVZ is believed to be thin or absent beneath India at the same location where very strong *PKP* scattering is observed. In addition to the ULVZs in the equatorial Pacific a relatively thick layer is found beneath central Africa where we infer strong scattering. A close correspondence between ULVZs and strong scattering might not be expected as high-velocity heterogeneity (such as the kind we expect lie beneath India) would not likely coexist with partial melt.

Tono and Yomogida [1996] analyzed *Pdiff*, the compressional phase that diffracts at the CMB, to study topography at this boundary. The existence of topographic irregularities at the CMB is inferred by the presence of a sequence of energetic short-period arrivals following *Pdiff*. They found evidence for a relatively smooth CMB north of Indonesia and a clear transition to a rougher CMB to the north along the Pacific rim. They found evidence for a rough CMB beneath India in a long north-south trend that extends to northern Eurasia. These trends of rugged CMB topography coincide with regions identified by our study as having stronger than average scattering. Similarly, we found weak scattering north of Indonesia where Tono and Yomogida infer a smooth CMB.

The correlation with the midmantle tomographic image in Plate 6 is imperfect. Although our inversion indicates strong scattering exists to the west of the Americas, there is no clear correlation between strong scattering in the deepest mantle and the Farralon trend which cuts diagonally across the Americas and is believed, at least in limited areas, to subduct to the deepest mantle [*van der Hilst et al.*, 1997]. Although a similar trend is seen in our inversion, there are some significant discrepancies. Central America, the location where *van der Hilst et al.* [1997] found evidence for penetration of the Farralon slab to the deepest mantle, is a region our inversion indicates has weaker than average scattering.

The idea that compositional heterogeneity may be important in the middle to lower mantle has been given new attention by the convection modeling and tomography analyses of *Kellogg et al.* [1999] and *van der Hilst and Karason* [1999]. These studies hypothesize that large topography exists on an undulating interface separating the midmantle from a chemically distinct and denser lower mantle. In downwelling regions this interface should be depressed closer to the core-mantle boundary in response to descending slabs in the midmantle. As discussed in section 5, our inversion for mantle scattering variations is for scale lengths of about 8 km, much smaller than those proposed for the topography on this interface. However, our results do indicate that the proposed lower layer, if it exists, is not compositionally uniform, because we observe strong scattering in the lowermost mantle beneath central Africa, a region removed from past subduction events.

6.4. Future Research Plans

Simple ray tracing shows that precursors from the deepest levels of the mantle arrive at the earliest times. Thus any study of *PKP* precursors will largely be a study of scattering in the lower mantle or at the CMB. The *PKP* data might be used to examine small-scale scattering structures above the lower mantle. Figure 1 and Plate 1 show that the amplitude increase with range seen in the precursors is accompanied by a similar amplitude increase in the coda. The range dependence seen in the *PKP* coda is clearly the result of small-scale scattering. Much of the scattering that gives rise to these late arrivals would have occurred at shallow depths, and thus the coda might be used to examine small-scale scattering in the middle to upper mantle.

The bootstrap test tells us that much of the mantle volume sampled by *PKP* precursors cannot be confidently identified as having anomalous small-scale scattering. The observations from the most heavily sampled region, northwest of Australia, are highly inconsistent (Figure 8), and some significant anomalies, such as the one beneath Tonga identified by *Vidale and Hedlin* [1998], are not clearly seen. In part, the results remain tentative and incomplete because of a lack of data. Further progress toward an accurate map of scattering intensity might come from an analysis of data from the GSN and other deployments such as those under the IRIS Program for Array Seismic Studies of the Continental Lithosphere (PASSCAL) program as well as the primary and secondary International Monitoring System seismic networks. Other networks, such as the Japanese Ocean Hemisphere Project, will include seismic stations on the ocean floor. These new deployments will allow us to image scattering patterns in areas that are currently not covered. Most global network stations record three components. An inversion that takes into account the particle motions as well as the travel times of the precursors may allow us to more effectively deal with the source-receiver ambiguity. This should reduce the data inconsistency problem and produce an image with more robust anomalies. However, the data inconsistency is not just due to incorrect energy partitioning. The *Vidale and Hedlin* [1998] study clearly demonstrates that extreme changes in the strength of scattering occur over small distances. A strong anomaly seen at a location such as the NORSAR array is not observed at a nearby GSN station. The true pattern of small-scale scattering in the mantle is highly aliased when analyzed using a sparse global network. This is a problem that no inversion method, even applied to three-component data, can overcome. Further progress on the fine detail of scattering in limited regions will come from analyses of global-regional integrated data. Dense deployments, such as those in the IRIS PASSCAL program, as well as broad aperture arrays such as NORSAR and the large-aperture seismic array (LASA) and regional networks such as the Kyrgyz broadband network (KNET) [*Vernon*, 1994] should shed light on the fine-scale structure in numerous areas.

Acknowledgments. This research was made possible by high-quality data in the FARM archive at the IRIS DMC. The authors would like to thank Ed Garnero and an anonymous reviewer for helpful comments. This research was funded by National Science Foundation grants EAR95-07994 and EAR96-28020.

References

Bataille, K., and S.M. Flatté, Inhomogeneities near the core-mantle boundary inferred from short-period scattered *PKP* waves recorded at the global digital seismograph network, *J. Geophys. Res., 93,* 15,057-15,064, 1988.

Bataille, K., and F. Lund, Strong scattering of short-period seismic waves by the core-mantle boundary and the *P*-diffracted wave, *Geophys. Res. Lett., 23,* 2413-2416, 1996.

Bijwaard, H., W. Spakman, and E.R. Engdahl, Closing the gap between regional and global travel time tomography, *J. Geophys. Res., 103,* 30,055-30,078, 1998.

Bolt, B.A., Gutenberg's early *PKP* observations, *Nature, 196,* 122-124, 1962.

Bullen, K.E., and T.N. Burke-Gaffney, Diffracted seismic waves near the *PKP* caustic, *Geophys. J. Int., 1,* 9-17, 1958.

Chernov, L.A. *Wave Propagation in a Random Medium,* (translated from the Russian by R.A. Silverman) 168 pp., McGraw-Hill, New York, 1960.

Christensen, U.R., and A.W. Hofmann, Segregation of subducted oceanic crust in the convecting mantle, *J. Geophys. Res., 99,* 19867-19884, 1994.

Cleary, J.R., and R.A.W. Haddon, Seismic wave scattering

near the core-mantle boundary: a new interpretation of precursors to *PKP*, *Nature, 240,* 549-551, 1972.

Cormier, V., Time domain modeling of *PKIKP* precursors for constraints on the heterogeneity in the lowermost mantle, *Geophys. J. Int., 121,* 725-736, 1995.

Cormier, V., Anisotropy of heterogeneity scale lengths in the lower mantle from *PKIKP* precursors, *Geophys. J. Int., 136,* 373-384, 1999.

Davies, G.F., Geophysical and isotopic constraints on mantle convection: An interim synthesis, *J. Geophys. Res., 89,* 6017-6040, 1984.

Doornbos, D.J., Characteristics of lower mantle inhomogeneities from scattered waves, *Geophys. J. R. Astron. Soc., 49,* 541-542, 1976.

Doornbos, D.J., On seismic-wave scattering by a rough core-mantle boundary, *Geophys. J. R. Astron. Soc., 53,* 643-662, 1978.

Doornbos, D.J., and E.S. Husebye, Array analysis of *PKP* phases and their precursors, *Phys. Earth Planet. Inter., 5,* 387, 1972.

Doornbos, D.J., and N.J. Vlaar, Regions of seismic wave scattering in the Earth's mantle and precursors to *PKP*, *Nature Phys. Sci., 243,* 58-61, 1973.

Dziewonski, A., and A.M. Anderson, Preliminary reference Earth model, *Phys. Earth Planet. Inter., 25,* 297-356, 1981.

Dziewonski, A.M., W.-J. Su, and R.L. Woodward, Grand structures of the Earth's interior (abstract), *Eos Trans. AGU, 72,* Fall Meet. Suppl., F451, 1991.

Efron, B., and R. Tibshirani, Statistical data analysis in the computer age, *Science, 253,* 390-395, 1991.

Garnero, E.J., and D.V. Helmberger, A very slow basal layer underlying large-scale low-velocity anomalies in the lower mantle beneath the Pacific: evidence from core phases, *Phys. Earth Planet. Inter., 91,* 161-176, 1995.

Garnero, E.J., and D.V. Helmberger, Seismic detection of a thin laterally varying boundary layer at the base of the mantle beneath the central-Pacific, *Geophys. Res. Lett., 23,* 977-980, 1996.

Grand, S.P., Mantle shear structure beneath the Americas and the surrounding oceans, *J. Geophys. Res., 99,* 11591-11621, 1994.

Gubbins, D., and R. Snieder, Dispersion of *P* waves in subducted lithosphere: evidence for an eclogite layer, *J. Geophys. Res., 96,* 6321-6333, 1991.

Gurnis, M., and G.F. Davies, Mixing in numerical models of mantle convection incorporating plate tectonics, *J. Geophys. Res., 91,* 6375-6395, 1986.

Gutenberg, B., and C.F. Richter, On seismic waves; I, *Gerlands Beitr. Geophysik., 43,* 56-133, 1934.

Gutenberg, B., The "boundary" of the Earth's inner core, *Eos Trans. AGU, 38,* 750-753, 1957.

Haddon, R.A.W., Corrugations on the CMB or transition layers between inner and outer cores? (abstract), *Eos Trans. AGU, 53,* 600, 1972.

Haddon, R.A.W., and J.R. Cleary, Evidence for scattering of seismic *PKP* waves near the mantle-core boundary, *Phys. Earth Planet. Inter., 8,* 211-234, 1974.

Hedlin, M.A.H., P.M. Shearer, and P.S. Earle, Imaging CMB scatterers through migration of GSN *PKPdf* precursor recordings (abstract), *Eos Trans. AGU, 76,* Fall Meet. Suppl., F402, 1995.

Hedlin, M.A.H., P.M. Shearer, and P.S. Earle, Seismic evidence for small-scale heterogeneity throughout the Earth's mantle, *Nature, 387,* 145-150, 1997.

Hestenes, M.R., and E. Stiefel, Methods of conjugate gradients for solving linear systems, *J. Res. Natl. Bur. Stand. U.S., 49,* 409-436, 1952.

Husebye, E.S., D.W. King, and R.A.W. Haddon, Precursors to *PKIKP* and seismic wave scattering near the mantle-core boundary, *J. Geophys. Res., 81,* 1870-1882, 1976.

Kaneshima, S., and G. Helffrich, Dipping low-velocity layer in the mid-lower mantle: Evidence for geochemical heterogeneity, *Science, 283,* 1888-1891, 1999.

Kellogg, L.H., B.H. Hager, and R.D. van der Hilst, Compositional stratification in the deep mantle, *Science, 283,* 1881-1884, 1999.

King, D.W., R.A.W. Haddon, and J.R. Cleary, Array analysis of precursors to *PKIKP*, in the distance range 128° to 142°, *Geophys. J. R. Astron. Soc., 37,* 157-173, 1974.

Loper, D.E., Mantle plumes, *Tectonophysics, 187,* 373-384, 1991.

Sacks, I.S., and G. Saa, The structure of the transition zone between the inner core and the outer core, *Year Book Carnegie Inst. Washington, 69,* 419-426, 1969.

Schmalzl, J., G.A. Houseman, and U. Hansen, Mixing in vigorous, time-dependent three-dimensional convection and application to Earth's mantle, *J. Geophys. Res., 101,* 21847-21858, 1996.

Shearer, P.M., M.A.H. Hedlin, and P.S. Earle, *PKP* and *PKKP* precursor observations: Implications for the small-scale structure of the deep mantle and core, *Geodynamics, 28,* 37-55, 1998.

Stacey, F.D., and D.E. Loper, The thermal boundary layer interpretation of D″ and its role as a plume source, *Phys. Earth Planet. Inter., 33,* 45-55, 1983.

Tono, Y., and K. Yomogida, Complex scattering at the core-mantle boundary observed in short-period diffracted *P*-waves, *J. Phys. Earth 44,* 729-744, 1996

van der Hilst, R.D., and H. Karason, Compositional heterogeneity in the bottom 1000 kilometers of Earth's mantle: Toward a hybrid convection model, *Science, 283,* 1885-1888, 1999.

van der Hilst, R.D., S. Widiyantoro, and E.R. Engdahl, Evidence for deep mantle circulation from global tomography, *Nature 386,* 578-584, 1997.

Vernon, F.L., The Kyrgyz seismic network, *IRIS Newslett., XIII(2),* 7-8, 1994.

Vidale, J.E., and M.A.H. Hedlin, Evidence for partial melt at the core-mantle boundary north of Tonga from the strong scattering of seismic waves, *Nature, 391,* 682-685, 1998.

Wen, L., and D.V. Helmberger, A two-dimensional *P-SV* hybrid method and its application to modeling localized structures near the core-mantle boundary, *J. Geophys. Res., 103,* 17901-17918, 1998.

Wen, L., S. Gao, P. Silver, and the Kaapvaal Working Group, Seismic structures in the lower mantle and the core-mantle boundary region beneath southern Africa (abstract), *Eos Trans. AGU, 79,* Fall Meet. Suppl., F579, 1998.

Williams, Q., J. Revenaugh, and E. Garnero, A correlation between ultra-low basal velocities in the mantle and hot spots, *Science, 281,* 546-549, 1998.

Wu, R.S., and K. Aki, Elastic wave scattering by a random medium and the small-scale inhomogeneities in the lithosphere, *J. Geophys. Res., 90,* 10261-10273, 1985.

M.A.H. Hedlin and P.M. Shearer, Institute of Geophysics and Planetary Physics, Scripps Institution of Oceanography, University of California, San Diego, La Jolla, CA 92093-0225. (e-mail: hedlin@ucsd.edu; pshearer@ucsd.edu

(Received May 21, 1999; revised November 15, 1999; accepted January 4, 2000.)